Point Cloud Semantic Segmentation Using a Deep Learning Framework for Cultural Heritage

Full-wave modeling of arcs within the ITER ICRF antenna for usage in the simulations and design of the RADAR Arc Detection system

Daniele Milanesio[1*], *Simone* Porporato[1], *Sara* Salvador[1], *Riccardo* Maggiora[1], *François* Calarco[2], *Walid* Helou[2], and *Kenji* Saito[2]

[1] Politecnico di Torino, Corso Duca degli Abruzzi 24, 10129 Torino, Italy
[2] ITER Organization, Route de Vinon-sur-Verdon, CS 90 046, 13067 St. Paul Lez Durance Cedex, France

Abstract. The ITER ICRF antenna [1] has been carefully designed to feature electrical fields below tolerable limits (typically, below 2 or 3 kV/mm depending on the location and orientation) when operating at a maximum voltage of 45 kV. In particular, this allows avoiding arcs. However, as for any high-power RF system, arcs can still occur in the ICRF antenna and its power feeding system, during normal operation and especially during the commissioning. Whenever an arc is detected, the RF power shall be immediately tripped (μs timescale) to avoid strong local energy deposition at the location of the arc. Undetected arcs are forbidden. To this aim, several complementary and redundant Arc Detection (AD) systems are foreseen to protect the ITER ICRF antenna. Among these AD systems is the RADAR Arc Detection (or RAAD [2]) which is currently under evaluation for implementation on the ITER ICRF system To provide a first numerical proof of concept of RAAD, full-wave simulations of the ITER ICRF antenna and its power feeding transmission lines have been performed in the radar bandwidth of operation (up to ~ 350 MHz) with the help of CST Studio Suite and ANSYS HFSS commercial codes. In these simulations, the plasma loading has been approximated by a salty water load (with a relative dielectric permittivity $\varepsilon_r = 80$ and electrical conductivity $\sigma = 1$ S/m), while arcs have been modelled with both perfect electric conductor (PEC) cylinders or lumped element shorts. The obtained S-matrices have been then loaded and processed by the RAAD time-domain circuit simulations and signal processing calculations 2. This paper describes the challenges to simulate the full ITER ICRF antenna with arcs, considering different loading conditions, different materials and different solutions for the arc insertion. It also provides a comparison of the scattering parameters with and without arcs.

1 Motivation and background

The ITER ICRF antenna [1] has been meticulously engineered to maintain electric field strengths below critical thresholds—typically under 2 to 3 kV/mm, depending on the specific location and orientation—when operating at its maximum voltage of 45 kV. This design goal helps to prevent arcing. Nevertheless, as is common with all high-power RF systems, arcs may still occur within the ICRF antenna or its power feeding system, especially during commissioning phases or even standard operation.

To mitigate the consequences of arcing, the RF power must be immediately interrupted upon arc detection (on the microsecond timescale), in order to prevent severe localized energy deposition (and the displacement of the arc along the system). The occurrence of undetected arcs is strictly unacceptable. For this reason, several complementary and redundant Arc Detection (AD) systems are planned for protecting the ITER ICRF antenna. Among them, the RADAR Arc Detection (RAAD) system [2] is quite promising, providing reliable detections and offering a unique feature such as precise localization of arcs and impairments. To provide an initial numerical proof of concept for RAAD, full-wave electromagnetic simulations of the ITER ICRF antenna and its associated transmission lines (TL) were conducted within the radar frequency range (up to ~350 MHz). We refer the interested reader to [2] for a detailed description of the RAAD system and to [3], [4] and [5] for some early work on the same subject, while we focus here on the full-wave simulations.

2 CST Studio Suite® modelling

All the results reported here were obtained using the commercial tool CST Studio Suite® [6]. CST Studio Suite® is a high-performance 3D EM analysis software package for designing, analyzing and optimizing electromagnetic (EM) components and systems. To be more specific, the Time Domain (TD) solver was selected for this analysis. The TD solver is a powerful and versatile multi-purpose transient 3D full-wave solver, with both finite integration technique and transmission line matrix implementations included in a single package. The TD solver can perform broadband simulations in a single run. CST Studio Suite® was installed on a GPU equipped machine to take advantage of the hardware acceleration option; the computing

* Corresponding author: daniele.milanesio@polito.it

machine is equipped with Intel Xeon ES-2695 v3 processors @2.30GHz, 128GB RAM and a NVIDIA Tesla K80 graphic card with 4992 cores.

It is also important to stress that, whenever feasible in terms of memory requirements, all results were also benchmarked with HFSS [7] (curves not shown here).

The ITER ICRF antenna front-face (see Fig. 1 and Fig. 2) and all the transmission line components were mainly simulated using a lossy metal (σ = 40e6 S/m); all simulations were also performed by setting all conductors to Perfect Electric Conductor (PEC). The plasma load in front of the ICRF antenna was approximated by a saline water model (εr = 80, σ = 1 S/m). Even though this choice of equivalent loading may not be a realistic plasma approximation for all the frequency range, it is important to stress that the RAAD algorithm is based on the differences between the system response with and without arcs; while a single simulation may be strongly affected by the loading, that difference is not. Arc faults were represented using either PEC cylinders or lumped-element shorts (0.001Ω). Boundary conditions all around the model were set to open, i.e. extending the material to infinity.

Three different loading scenarios were taken into account, moving the plasma load from 0 mm, to 50 mm and eventually to 110 mm from the antenna, and filling the remaining gap with vacuum. Fig. 1 and Fig. 2 show a front and a side view of the ITER ICRF antenna front-face, respectively.

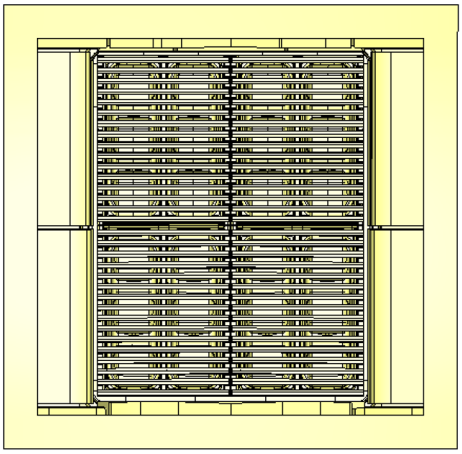

Fig. 1. Front view of the ITER ICRF antenna front-face. All metallic surfaces have been represented using a lossy metal (σ = 40e6 S/m).

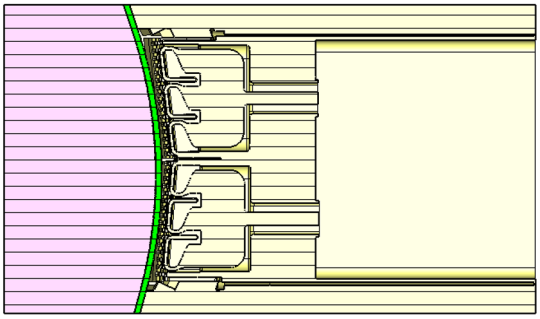

Fig. 2. Side cross section of the ITER ICRF antenna front-face. The load (in pink in the picture) is a saline water model (ε_r = 80, σ = 1 S/m), which is separated from the antenna by a variable vacuum layer (in green in the picture), going from 0 mm to 110 mm.

A first batch of simulations was performed to assess the influence of the mesh and of the water load radial extension at the IC frequency range. The optimized geometry was then simulated on the full RAAD range (30÷400 MHz), requiring a mesh of about 315M unknowns, and taking slightly more than 20 hours on our GPU-based machine.

2.1 Simulation challenges

Because of the geometrical complexity of the ITER ICRF antenna and TL, the raw S matrices were affected by oscillations, which were caused by the presence of a certain amount of energy left in the structure at the end of the time domain transient simulation. According to CST Studio Suite®, this inconvenience can be mitigated by increasing the simulation accuracy or by applying an embedded autoregressive filter (ARF), which still requires optimization. However, despite the usage of the ARF and a reduction of about 5% of the non-passive frequency points, S matrices were still not passive on the entire frequency range. It must be stressed that the non-passivity in the frequency domain CST Studio Suite® simulations determined a divergence in the time domain RAAD algorithm in a very precise point. This allowed us to discard it completely and, hence, to obtain very good agreement between the arc position estimated by the RAAD and its exact location in the full-wave simulations. Fig. 3 compares the raw data obtained from one of the CST Studio Suite® simulations with the ones obtained with the usage of the ARF.

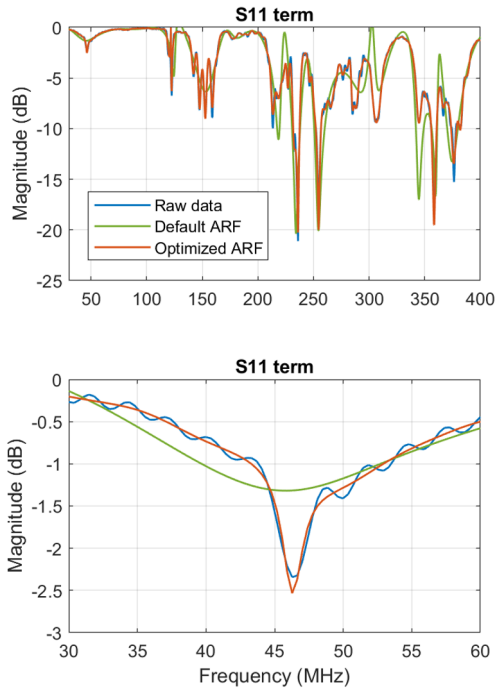

Fig. 3. Comparison between the raw scattering matrix trace (in blue), the curve obtained applying the default AR filter (in green) and the one with the optimized ARF (in red). The entire RAAD frequency range is depicted on top, while a zoomed view of the IC frequencies is reported below.

3 Analysis of the ITER ICRF launcher

As a first attempt, a PEC cylinder of 1 mm diameter was inserted into the simulation to mimic the arc behaviour. Even though this additional element determined only a slight increase of the meshed elements (from about 316M to 323M), the simulation time jumped from about 19 hours to 97 hours. This is linked to time-step adopted by the solver, i.e. the speed at which the signal is propagated in the computational volume: the smaller the mesh size, the smaller the time-step needs to be, the longer the simulation time is. To be more specific, the smallest mesh element moved from 3 mm to 0.5 mm with the insertion of the cylinder.

On the contrary, the insertion of a lumped element did not affect the mesh and, hence, the simulation time, still providing a very good agreement with respect to the PEC cylinder.

Fig. 4 shows the position of the simulated arcs. It is important to mention that all arcs were located within the first triplet (see picture inset in the bottom right), corresponding to the upper left port in the TL system.

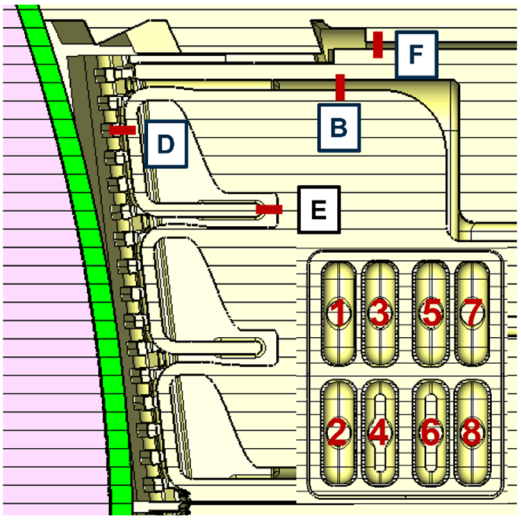

Fig. 4. Side view of the first triplet (top left corner of the antenna seen from the back) with the location of the simulated arcs.

Fig. 5 and Fig. 6 report some entries of the 8x8 scattering matrix simulated, with a specific focus on the frequency range where the RAAD system will operate.

The reader can immediately notice that the presence of an arc (an arc in position D in the proposed example) significantly affects the S_{1X} terms of the scattering matrix, i.e. the row corresponding to the couplings to the first triplet. Fig. 6 points out that, while the arc can still affect port 3 (next toroidal neighbour), there is no relevant contribution when looking at port 8, i.e. at the opposite corner of the antenna.

As an example of the RAAD output, Fig. 7 shows the detection of the arcs located in the antenna region. The peak in the signal correlation (see [2] for a detailed explanation of the involved algorithm and the description of all available results) indicates the presence of an arc. The zoomed view points out that the exact position of the arc can be computed within a few centimetres of error.

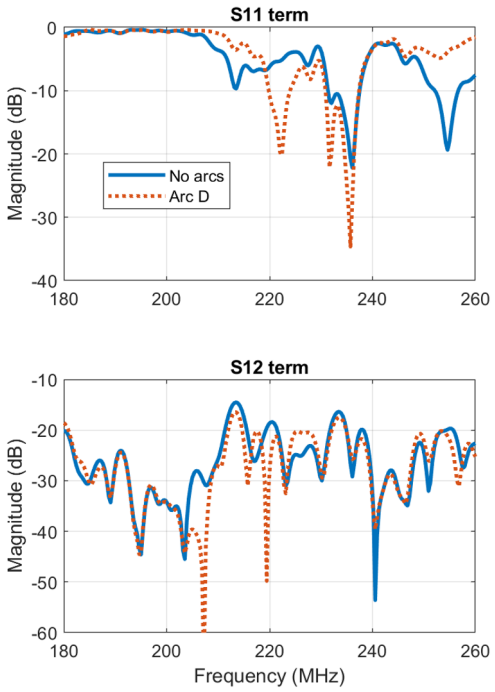

Fig. 5. Comparison between the simulated scattering matrix in case of no arcs (blue curve) and in case of arc located in position D on the first triplet (dotted red curve). Only two entries of the full 8x8 matrix are shown for simplicity and the plot is limited to the working frequency of the RAAD.

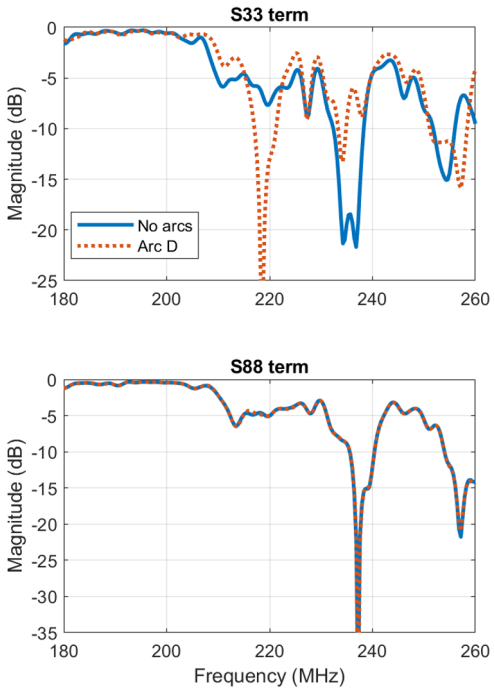

Fig. 6. Comparison between the simulated scattering matrix in case of no arcs (blue curve) and in case of arc located in position D on the first triplet (dotted red curve). Only two entries of the full 8x8 matrix are shown for simplicity and the plot is limited to the working frequency of the RAAD.

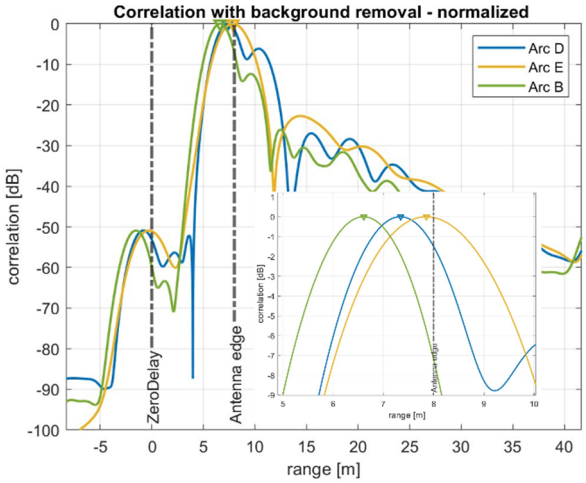

Fig. 7. Correlation plot obtained by the RAAD system with zoomed view of the peaks. A peak in the correlation indicates the presence of an arc, which can also be precisely located in range as shown by the magnified inset.

Arcs in the cavity surrounding the antenna can also be detected (i.e. arc F in Fig. 4), but the localization is currently not possible via modelling. At the range of the antenna the radar response shows a global change, indicating the presence of an event, but there is not a clear peak, which is needed to determine the location of the arc.

4 Analysis of the ITER ICRF antenna feeding transmission lines

To conclude the full-wave analysis with CST Studio Suite®, several parts of the ITER antenna transmission lines were simulated, first without arcs, then including arcs in different strategical positions, in the frequency range 30÷400 MHz. In this case, arcs were inserted through PEC cylinders only. For instance, in Fig. 8, which represents the portion of the ITER TL simulated, one can notice arcs located in "random" positions (in red), in the low voltage points (in light blue), at the voltage nodes at 55 MHz (in green), in series (in violet). Together with arcs, also metallizations on ceramic materials were taken into account (in yellow).

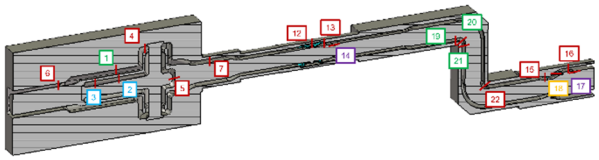

Fig. 8. Transmission line section simulated with CST Studio Suite® and position of the arcs.

Fig. 9 and Fig. 10 show a detailed view of the service stub area (located right before, source-side, of the antenna front-face) and of the rear window, respectively.

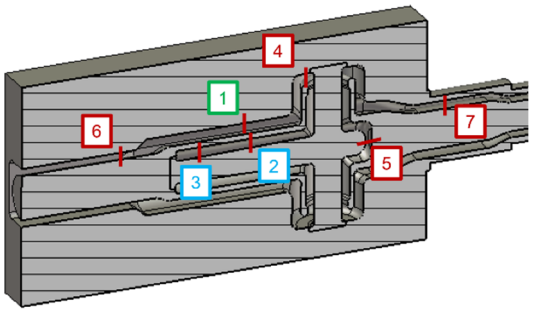

Fig. 9. Detailed view of the last part of the TL, right before the four port junction, and arc positions. Green number corresponds to an arc located at voltage nodes at 55 MHz while blue numbers indicate arcs in low voltage positions.

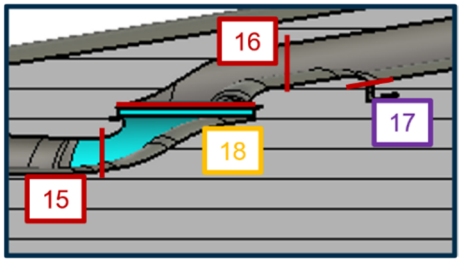

Fig. 10. Detailed view of the rear window of the TL. Yellow numbers correspond to metallization on top of a ceramic component while violet ones are series arcs.

Given the positions of the arcs depicted in Fig. 9, Fig. 11 documents the impact on the scattering matrix; all arcs are clearly visible. Fig. 12 shows the same figure of merit for the arcs indicated in Fig. 10; this time, the curve corresponding to the series arc 17 seems to be perfectly overlapped to the reference case. However, the two curves are separated by about 0.02 dB.

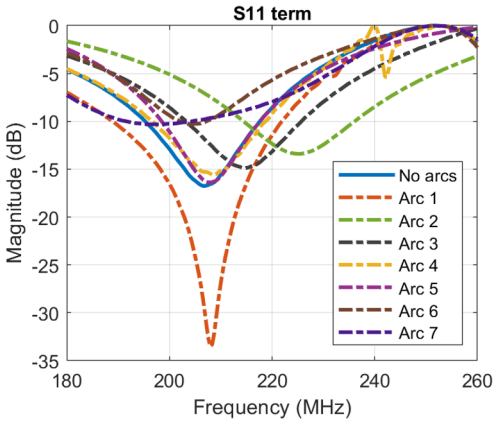

Fig. 11. Comparison between the simulated scattering matrix in case of no arcs (blue curve) and in case of arcs located in several different positions shown in Fig. 9 on the TL (dotted curves).

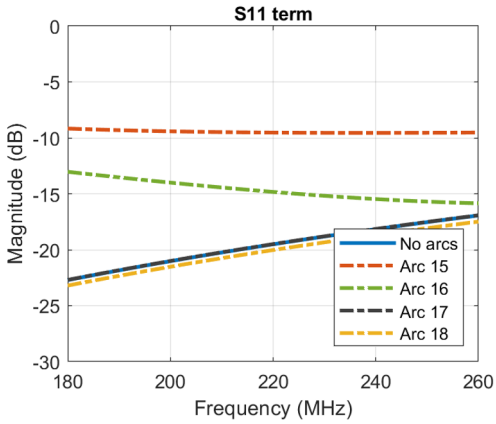

Fig. 12. Comparison between the simulated scattering matrix in case of no arcs (blue curve) and in case of arcs located in several different positions shown in Fig. 10 on the TL (dotted curves).

As done for the ITER ICRF launcher, an example of detection and arc localization for the two sets of arcs is reported in Fig. 13 and Fig. 14. Please notice that the RAAD takes into account through analytical models also parts of the feeding lines that were not simulated with CST Studio Suite®.

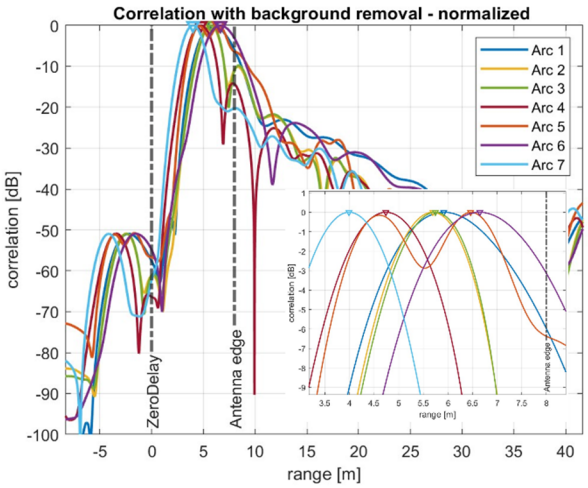

Fig. 13. Correlation plot obtained by the RAAD system with zoomed view of the peaks. A peak in the correlation indicates the presence of an arc, which can also be precisely located in range as shown by the magnified inset.

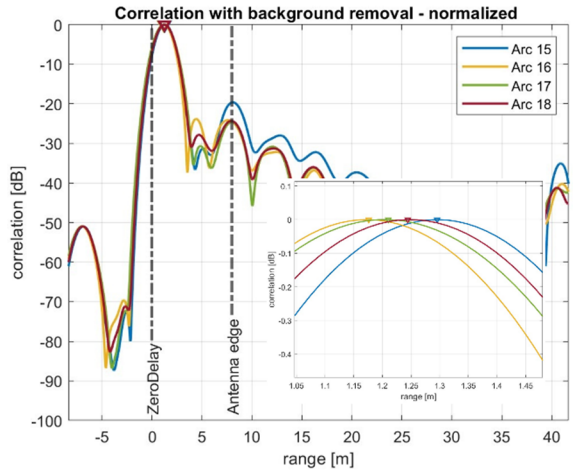

Fig. 14. Correlation plot obtained by the RAAD system with zoomed view of the peaks. A peak in the correlation indicates the presence of an arc, which can also be precisely located in range as shown by the magnified inset.

5 Conclusions

The presence of arcs and impairments both in the launcher and in the TL components of ITER ICRF system can be reliably simulated with CST Studio Suite® up to the radar frequency range. The calculated S matrices clearly indicate the presence of arcs and they can be effectively used in the radar time domain simulation. This allows to verify radar performances in terms of detection, localization, and classification of all arcs everywhere, including low voltage regions.

To provide a further validation of the RAAD in the real environment, our next steps foresee the assembly of a prototype and the installation and testing in ASDEX upgrade during plasma operation.

This work has been conducted under contract IO/24/CT/4300003010. The views and opinions expressed herein do not necessarily reflect those of the ITER Organization.

References

1. W. Helou et al., The ITER ICRF system under the new ITER baseline: latest updates and technological developments, 25th Topical Conference on Radio-Frequency Power in Plasmas, Schloss Hohenkammer, Germany, May 19-22 (2025), https://www.ipp.mpg.de/5487515/Talks
2. S. Porporato et al., Radar arc and impairment detection and localization for the ITER ICRF antenna, 25th Topical Conference on Radio-Frequency Power in Plasmas, Schloss Hohenkammer, Germany, May 19-22 (2025), https://www.ipp.mpg.de/5487515/Talks
3. R. Maggiora, S. Salvador, UWB radar technique for arc detection in coaxial cables and waveguides, AIP Conf. Proc. **1187**, 261–264 (2009). https://doi.org/10.1063/1.3273743
4. S. M. Salvador, R. Maggiora, R. D'Inca, H. Fuenfgelder, Arc Detection With GUIDAR: First Experimental Tests On MXP Testbed, AIP Conf. Proc. **1406**, 25–28 (2011). https://doi.org/10.1063/1.3664921
5. S. M. Salvador, R. Maggiora, R. H. Goulding, J. A. Moore, R. I. Pinsker, A. Nagy, Guided radar system for arc detection: Initial results at DIIID. AIP Conf. Proc. **1580**, 283–286 (2014). https://doi.org/10.1063/1.4864543
6. https://www.3ds.com/products/simulia/cst-studio-suite
7. https://www.ansys.com/it-it/products/electronics/ansys-hfss